American Journal of Botany 94(8): 1371–1381. 2007.

AERODYNAMICS OF SACCATE POLLEN AND ITS IMPLICATIONS FOR WIND POLLINATION[1]

ANDREW B. SCHWENDEMANN,[2,5] GEORGE WANG,[3] MEREDITH L. MERTZ,[2] RYAN T. MCWILLIAMS,[2] SCOTT L. THATCHER,[3] AND JEFFREY M. OSBORN[2,4,6]

[2]Division of Science, Truman State University, Kirksville, Missouri 63501-4221 USA; and
[3]Division of Mathematics and Computer Science, Truman State University, Kirksville, Missouri 63501-4221 USA

Pollen grains of many wind-pollinated plants contain 1–3 air-filled bladders, or sacci. Sacci are thought to help orient the pollen grain in the pollination droplet. Sacci also increase surface area of the pollen grain, yet add minimal mass, thereby increasing dispersal distance; however, this aerodynamic hypothesis has not been tested in a published study. Using scanning electron and transmission electron microscopy, mathematical modeling, and the saccate pollen of three extant conifers with structurally different pollen grains (*Pinus*, *Falcatifolium*, *Dacrydium*), we developed a computational model to investigate pollen flight. The model calculates terminal settling velocity based on structural characters of the pollen grain, including lengths, widths, and depths of the main body and sacci; angle of saccus rotation; and thicknesses of the saccus wall, endoreticulations, intine, and exine. The settling speeds predicted by the model were empirically validated by stroboscopic photography. This study is the first to quantitatively demonstrate the adaptive significance of sacci for the aerodynamics of wind pollination. Modeling pollen both with and without sacci indicated that sacci can reduce pollen settling speeds, thereby increasing dispersal distance, with the exception of pollen grains having robust endoreticulations and those with thick saccus walls. Furthermore, because the mathematical model is based on structural characters and error propagation methods show that the model yields valid results when sample sizes are small, the flight dynamics of fossil pollen can be investigated. Several fossils were studied, including bisaccate (*Pinus*, *Pteruchus*, *Caytonanthus*), monosaccate (*Gothania*), and nonsaccate (*Monoletes*) pollen types.

Key words: aerodynamic efficiency; anemophily; computational model; fossil pollen; mathematical model; palynology; pollen; saccate pollen; wind pollination.

Pollination in seed plants can be accomplished by either biotic or abiotic means. Biotic pollination can be facilitated by a variety of animals; abiotic pollination typically involves pollen transfer by either wind or water. Wind pollination is commonly thought to be a random and metabolically wasteful process, in which copious amounts of pollen are produced and released (Niklas, 1985b). The pollen-to-ovule ratio for wind-pollinated taxa can be orders of magnitude greater than that for insect-pollinated plants (Niklas, 1992). This larger energy investment may be offset by a lack of showy petals, a lack of nectaries, and no consumption of pollen by an animal vector (Dowding, 1987). A range of studies undertaken in the last twenty-five years has shown that wind pollination is more efficient than traditionally thought (Niklas, 1987). These studies have demonstrated that the efficiency of wind pollination is influenced by the aerodynamics of various plant parts that work together to increase the probability of pollen entrapment on the ovulate organs.

The Coniferophyta is one group that has been extensively studied for aerodynamic efficiency, likely due to the prevalence of wind pollination in conifers (Crane, 1986). The morphology of ovulate cones is such that airborne pollen is aerodynamically directed through the scales to the pollination droplet (Niklas and Paw U, 1983). Through this process, ovulate cones are able to partially filter-out pollen of non-conspecific taxa (Niklas and Paw U, 1982; Niklas, 1984, 1985b). In addition, the fascicles surrounding ovulate cones of some *Pinus* species deflect airborne pollen toward the cones by creating turbulent wakes (Niklas, 1984, 1985a). Moreover, the harmonic motion of branches bearing ovulate cones may increase the efficiency of wind pollination (Niklas, 1985a).

The morphology of pollen grains may also affect the aerodynamics of wind pollination. Pollen vectored by animals is often structurally different than pollen dispersed by wind (Osborn et al., 1991). In conifer pollen, the gametophytic cells are housed in a spheroidal main body, protected by a two-layered pollen wall. The inner layer, or intine, is composed mainly of cellulose. The outer layer, or exine, is composed of sporopollenin. In many conifers, the exine expands outward from the main body to form one to three air-filled bladders, or sacci. A long-standing perspective is that sacci help to orient pollen grains in the pollination droplet to facilitate pollination (Doyle and O'Leary, 1935), and recent studies have supported this early hypothesis (Tomlinson, 1994; Runions et al., 1999; Salter et al., 2002). Although sacci appear to aid pollen orientation within the pollination droplet, Wodehouse (1935) proposed that sacci play a role in the aerodynamics of pollen as well. Sacci increase the surface area of the grains, while ideally adding a minimum of mass. This, in turn, increases the amount of drag on pollen grains. Increased drag reduces the settling speed of pollen, causing dispersal distances to increase. Because settling speeds are proportional to mass and density,

[1] Manuscript received 3 November 2006; revision accepted 26 June 2007.

The authors thank I. M. Lindevald (Truman State University) for contributions to the initial computational model, as well as T. Barcus and T. W. Sorrell (Truman State University) for their help with stroboscopic photography experiments. The authors also thank the Missouri Botanical Garden for a loan of herbarium material. This study was supported in part by Truman State University and the National Science Foundation (DUE-0337760 and DUE-0436348).

[4] Author for correspondence (e-mail: josborn@tcnj.edu)

[5] Current address: Department of Ecology and Evolutionary Biology, University of Kansas, Lawrence, Kansas 66045 USA

[6] Current address: School of Science, The College of New Jersey, Ewing, New Jersey 08628 USA

smaller pollen grains will also travel farther. However, because of the low momentum of such small pollen grains, such grains may have difficulty breaking through the boundary layer of air to land on ovulate cones (Whitehead, 1983; Niklas, 1985a). No published studies, however, have investigated the aerodynamic properties of saccate pollen grains.

Saccate pollen occurs in three families of extant conifers: Pinaceae, Podocarpaceae, and Phyllocladaceae. The sacci in members of the Phyllocladaceae are thought to possibly be vestigial and nonfunctioning. Saccate pollen is also found in numerous extinct groups (Osborn and Taylor, 1994; Tomlinson, 2000), including seed ferns (Callistophytales, Glossopteridales, Corystospermales, Caytoniales) and conifers (Cordaitales, Voltziales).

The objectives of this study were to empirically and computationally verify the effects of sacci in the wind dispersal of saccate pollen grains and to develop a valid, mathematical model of pollen settling speeds that can substitute for empirical testing. The mathematical model, based on structural characters, permits flight properties to be measured without physically testing pollen, allowing the flight dynamics of fossil pollen to be investigated. The pollen grains used in this study were chosen because of their structural variability in overall size, saccus size, amount of endoreticulations, and surface ornamentation.

MATERIALS AND METHODS

Pollen material—Pollen of *Pinus strobus* L. and *Pinus mugho* Turra (Pinaceae) was gathered from trees located on the campus of Truman State University. *Pinus sylvestris* L. pollen was collected from a private residence in Kirksville, Missouri, USA. Pollen of *Zea mays* L. (Poaceae) was gathered from the Truman State University greenhouse. Pollen from *Dacrydium franklinii* Hook. and *Falcatifolium taxoides* (Brongn. & Gris) de Laub. (Podocarpaceae) was gathered from herbarium specimens on loan from the Missouri Botanical Garden. Structural data from all fossil pollen and extant *Abies* were obtained from the published literature: *Gothania lesliana* (Hirmer) Daghlian et Taylor (Cordaitales; Taylor and Daghlian, 1980), *Caytonanthus arberi* (Thomas) Harris (Caytoniales; Osborn, 1994), *Monoletes* pollen from *Dolerotheca formosa* Shopf (Medullosales; Taylor, 1978), *Pteruchus fremouwensis* Yao, Taylor, and Taylor (Corystospermales; Osborn and Taylor, 1993), a fossil *Pinus* sp. (Coniferales; Phipps et al., 1995), and *Abies concolor* (Gord. & Glend.) Lindl. ex Hildebr. (Pinaceae; Kurmann, 1989).

Microscopy—Dehiscent and near-dehiscent pollen cones of *Pinus strobus* were cut into sections using a razor blade. Fragments of dehiscent *Dacrydium franklinii* and *Falcatifolium taxoides* cones were removed from herbarium sheets and encased in agar blocks before sample preparation.

For studying pollen ultrastructure, the samples were dehydrated in a series of ethanol and acetone rinses and were then gradually infiltrated and embedded in Spurr's epoxy resin (Electron Microscopy Sciences, Fort Washington, Pennsylvania, USA). The embedded specimens were thick- and thin-sectioned with an RMC MT-6000XL ultramicrotome (Tucson, Arizona, USA) using glass and diamond knives. Thick-sections (850 nm) were collected on glass slides, stained with Richardson's stain (azure II and methylene blue), and viewed with bright-field microscopy on an Olympus (Lake Success, New York, USA) BHS compound light microscope to determine whether the pollen grains were fully mature. Thin-sections (70–90 nm) were collected and dried on formvar-coated copper slot grids and were stained with 1% uranyl acetate, lead citrate, and 1% potassium permanganate. Pollen was examined and imaged using a JEOL (Peabody, Massachusetts, USA) JEM-100SX transmission electron microscope (TEM) at 60–80 kV.

For documenting external pollen characters, dissected cone samples were gradually dehydrated in ethanol and critical point dried. Dried cone material was transferred to a glass microscope slide where the sample was macerated with a syringe needle to expose the pollen. Pollen grains were then mounted on aluminum stubs using double-sided tape. The stubs were sputter-coated with gold-palladium and examined and imaged using a JEOL JSM-6100 scanning electron microscope (SEM) at 5 kV.

Mathematical model—A structurally based mathematical model of pollen flight was created to study the aerodynamic features of pollen grains. The model was designed to output the settling speed of a single pollen grain, using various structural measurements and physical constants as its input. The model was constructed on the assumption that the main body and sacci of the pollen grain are each a prolate spheroid. The equation used to describe the main body of the pollen grain is that of an ellipsoid:

$$(x^2/C^2) + (y^2/B^2) + (z^2/A^2) = 1, \tag{1}$$

where x, y, and z are the surface coordinates for the ellipsoid and A, B, and C are the lengths of the semi-axes of the ellipsoid. The equation used to describe the sacci is that of an ellipsoid that has been rotated and translated from the origin in order to describe the position of the sacci in relation to the main body of the pollen grain:

$$\frac{(x-x_0)^2}{c^2} + \frac{[(y-y_0)\cos(\theta) + (z-z_0)\sin(\theta)]^2}{b^2} + \frac{[(z-z_0)\cos(\theta) - (y-y_0)\sin(\theta)]^2}{a^2} = 1, \tag{2}$$

where (x_0, y_0, z_0) is the center of the translated ellipsoid; θ is the angle between the long axis of the ellipse and the horizontal axis of the coordinate plane; and a, b, and c are the lengths of the semi-axes of the ellipsoid.

The total force acting on the pollen grain is the sum of the downward force of gravity and the upward drag force. At terminal velocity, where acceleration is zero, the sum of the two forces is zero. Therefore, under these circumstances, the magnitude of the force of gravity is equal to the magnitude of the force of drag. The force applied to the pollen grain due to gravity is equal to the product of the mass m of the grain and the acceleration g due to gravity. In the mathematical model, drag is defined as the product of the grain's velocity U_S, the viscosity μ of air, the cube root of the volume V, and a drag coefficient C_D (Vogel, 1994). Setting these two forces equal gives:

$$mg = U_S C_D V^{1/3} \mu, \tag{3}$$

and solving for the terminal velocity U_S gives:

$$U_S = (mg)/C_D V^{1/3} \mu. \tag{4}$$

The drag coefficient, C_D, depends on the shape of the object moving through the fluid and determines the constant of proportionality between $V^{1/3}$ and the drag force. To determine C_D, the overall shape of the pollen grain was assumed to be spheroid. The coefficients for drag used in the model were derived from standard drag coefficients for various prolate and oblate spheroids (Vogel, 1994).

Structural characters and development of the mathematical model—The variables from Eq. (4) that need to be determined are the volume, mass, and drag coefficient of each pollen grain. Numerous structural characters of the pollen grains were measured to determine these variables (Figs. 1–15). Lengths and angles of these characters were measured from SEM micrographs, and ultrastructural characters were measured from TEM micrographs (Table 1). Micrographs were measured using ImageJ image analysis software (National Institutes of Health, Bethesda, Maryland, USA; ImageJ, 2004).

Volume—Length and angle measurements from SEM micrographs were used to determine the volume of the pollen grain. For the actual measurements, an ellipse was fitted to each of the sacci and to the main body (Fig. 16). The long and short axes of all ellipses were measured in the equatorial view of the pollen grain. The axis length of the third dimension of the ellipsoid was an averaged measurement taken from micrographs of pollen grains in proximal view. The angle of rotation of the sacci and the distance from the center of the main body to the center of the sacci were measured from micrographs showing pollen grains in equatorial view. This method created an overlap between each saccus and the main body (Fig. 16). The volume of this overlap was determined using Monte Carlo integration (Press et al., 1986), and the overlap was subtracted from the initial, overestimated saccus volume. Expressed mathematically:

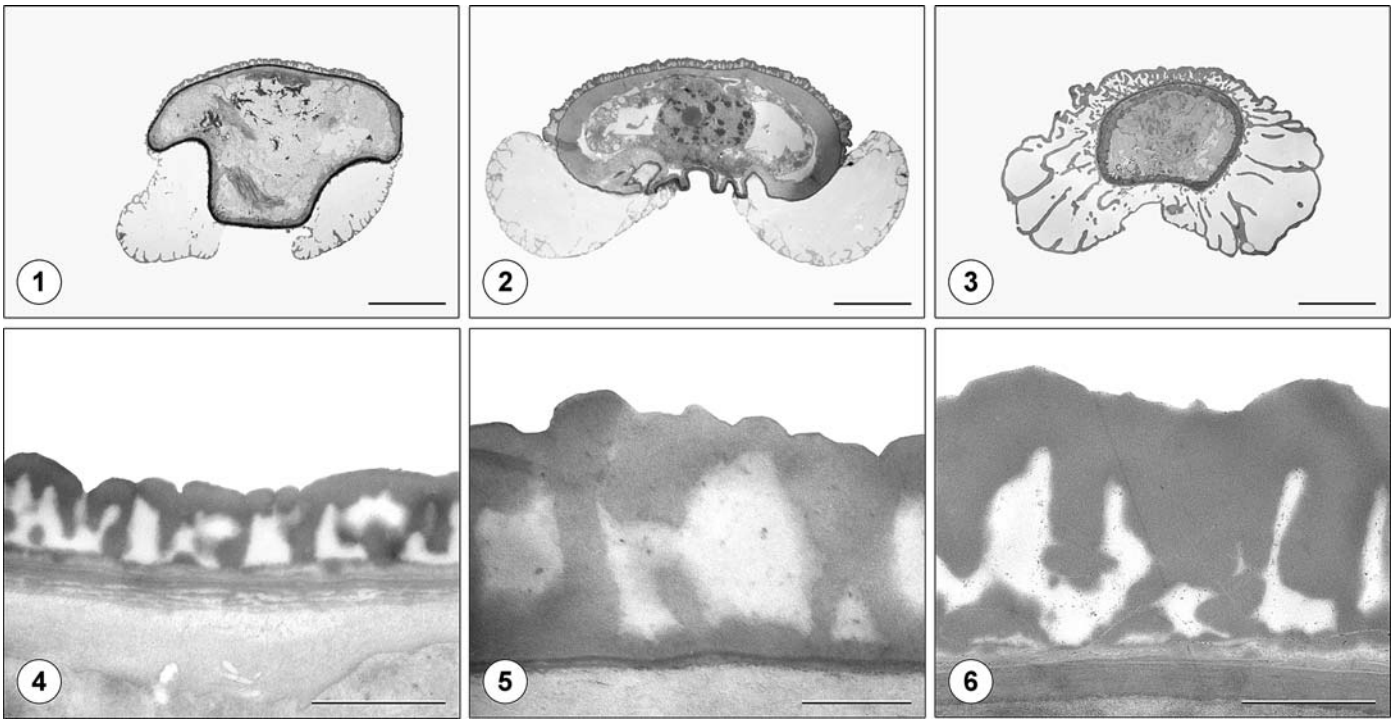

Figs. 1–6. Transmission electron micrographs showing pollen ultrastructure of the three extant grain types used to create the mathematical model. Equatorial section through a pollen grain of **1.** *Dacrydium franklinii*, **2.** *Pinus strobus*, and **3.** *Falcatifolium taxoides*, bars = 10 μm. Section through the proximal wall of a pollen grain of **4.** *D. franklinii*, bar = 1.0 μm, **5.** *P. strobus*, bar = 0.5 μm, and **6.** *F. taxoides*, bar = 1.0 μm.

$$V_{\text{sac}} = V_{\text{ellipsoid}} - V_{\text{overlap}}, \tag{5}$$

where V_{sac} is the corrected saccus volume, $V_{\text{ellipsoid}}$ is the volume of the saccus ellipsoid, and V_{overlap} is the volume of overlap between the saccus and the main body.

Mass—Ultrastructural measurements taken from TEM micrographs (Fig. 17) were used in conjunction with measurements from SEM micrographs to calculate the mass of the pollen grains. The ultrastructural data for each character were averaged from numerous grains, and those averages were used with individual SEM measurements to produce settling speeds. Thicknesses of the pollen grain exine and intine were determined by averaging thicknesses measured at regular intervals along the pollen walls. The proximal exine walls were measured so that only the exine was included in the volume calculations. These average thicknesses were then used along with the total volume measurement of the main body to determine the individual volumes of the exine, intine, and living cells. The volumes of the layers were then multiplied by their respective densities to determine the masses of the layers (protoplasm: 0.998 g/cm^3, Niklas, 1985a; sporopollenin: 1.27 g/cm^3, Southworth, 1988; cellulose: 1.36 g/cm^3, Wayne and Staves, 1991). For example, the volume of an ellipse is $(4/3)\pi abc$, where a, b, and c are the lengths of the semi-axes. The mass of the main body exine would then be approximated by:

$$m_{\text{exine}} = \rho_{\text{sporopollenin}}[(4/3)\pi abc - (4/3)\pi(a - \tau_{\text{exine}})(b - \tau_{\text{exine}})(c - \tau_{\text{exine}})], \tag{6}$$

where τ is used to denote the thickness of layers in the pollen grain and ρ represents density. The mass of cellulose was calculated in the same manner. The mass of living cells was not calculated using a measured thickness. For the living cells, the remaining volume of the ellipse not taken up by the exine or intine was used to determine the volume.

The mass of the saccus wall was determined similarly, again using Monte Carlo integration to determine the overlap of the main body with the saccus wall:

$$m_{\text{saccus wall}} = \rho_{\text{sporopollenin}}\{[(4/3)\pi abc - (4/3)\pi(a - \tau_{\text{wall}})(b - \tau_{\text{wall}})(c - \tau_{\text{wall}})] - V_{\text{wall overlap}}\}. \tag{7}$$

Determining the mass of endoreticulations in the sacci required a different method. Endoreticulations are extensions of the exine inside the saccus cavity, forming a honeycomb-like mesh (Fig. 18). The amount and size of these endoreticulations vary from species to species. For finding the mass of the endoreticulations, representative regions were selected from a TEM micrograph of an equatorial section (Fig. 17). These regions extended into the sacci to a distance equal to the depth of the endoreticulation layer. The area of the endoreticulations and the total area of the section being considered were used to calculate the percentage ε of endoreticulations in a given area. The average depth τ_{endo} that the endoreticulations extend into the sacci was then measured. That depth, along with the percentage of endoreticulations in a given section and the volume measurements derived from SEM data, was used to calculate the volume of endoreticulations present. The mass of the endoreticulations was then determined as:

$$m_{\text{endo}} = \varepsilon\rho_{\text{spor}}\{[(4/3)\pi(a - \tau_{\text{wall}})(b - \tau_{\text{wall}})(c - \tau_{\text{wall}})] - [(4/3)\pi(a - \tau_{\text{endo}})(b - \tau_{\text{endo}})(c - \tau_{\text{endo}})]\} - \varepsilon\rho_{\text{spor}}V_{\text{endo overlap}}, \tag{8}$$

where $V_{\text{endo overlap}}$ is the volume of overlap between the main body and the endoreticulation layer, and a, b, and c are the lengths of the saccus ellipsoid axes.

Figures 19–21 demonstrate the fit of the modeled pollen grain to the actual measured grain.

Drag coefficient—The drag on a spheroid depends on the ratios of its length, width and height and on its orientation relative to its direction of motion. On the basis of the stroboscopic photography experiments described later, the bisaccate pollen grains were assumed to be oriented with the sacci facing upward/backward, relative to the wind direction, during their descent. The drag

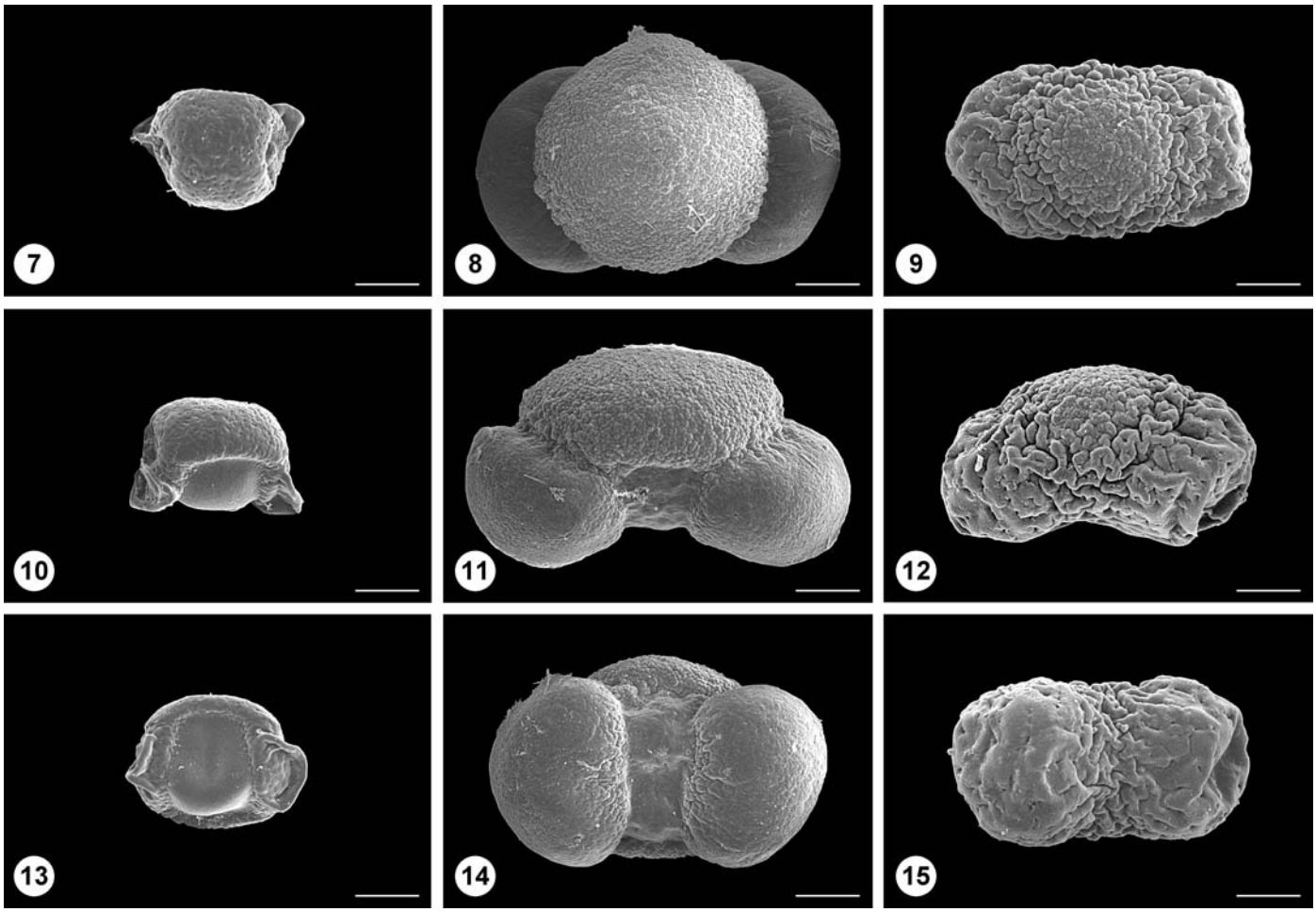

Figs. 7–15. Scanning electron micrographs showing pollen morphology of the three extant grain types used to create the mathematical model. Proximal view of a pollen grain of **7.** *Dacrydium franklinii*, **8.** *Pinus strobus*, and **9.** *Falcatifolium taxoides*, bars = 10 μm. Equatorial view of a pollen grain of **10.** *D. franklinii*, **11.** *P. strobus*, and **12.** *F. taxoides*, bars = 10 μm. Distal view of a pollen grain of **13.** *D. franklinii*, **14.** *P. strobus*, and **15.** *F. taxoides*, bars = 10 μm.

coefficient was determined using dimensions for the length-to-width ratio taken from pollen grains in both the equatorial and proximal views. An averaged width was taken from numerous pollen grains in proximal view. The length used to determine the drag coefficient was measured individually for each pollen grain in equatorial view. The length was defined as the distance from the end of one saccus to the end of the other saccus.

Modeling fossil pollen—The seed fern *Caytonanthus* is known from compression fossils, whereas all other fossils in this study are known from permineralizations. Although the exine generally preserves well through the fossilization process, the intine and the once living cells do not. As a result, it was necessary to estimate the thickness of the intine. As such, the intine thicknesses of similar-sized pollen grains from an allied, extant relative were used. For *Caytonanthus* (Figs. 22, 23), *Monoletes* (Figs. 32, 33), and *Pteruchus* (Figs. 27, 30), intine data from *Zamia* were used (Zavada, 1983); for fossil *Pinus* (Figs. 28, 31), data from extant *Pinus* from this study were used (Table 1); and for *Gothania* (Figs. 26, 29), intine data from *Picea* were used (Runions et al., 1999).

Permineralized pollen grains—All the permineralized fossils were assumed to have been preserved in such a manner that their three-dimensional structure has been preserved and can be used to make accurate measurements.

Mathematical expansion of compressed pollen grains—*Caytonanthus* pollen (Figs. 22, 23) was "expanded" by measuring the grain's main body and saccus cross-sectional circumferences and using ellipsoids of the same cross-sectional circumference in the model. Because of the resistant nature of sporopollenin, the cross-sectional circumference was assumed to be preserved in compression. These circumferences were measured from SEM micrographs using the program ImageJ (ImageJ, 2004). Prolate spheroids with the same cross-sectional circumferences were found and used to model the pollen grain using Ramanujan's approximation equation (Almkvist and Berndt, 1988). Dimensions of the three spheroids were then used in the model to determine the settling speed.

The displacements of the sacci from the main body were estimated using extant pollen grains as a guide because the actual values could not be deduced from the compression. The degree of overlap of the sacci and the main body varied depending on the estimated values of saccus displacement. For determining the effect that estimating the displacement of the sacci had on the grain, the model was run under two scenarios in which the amount of overlap differed (Figs. 24, 25).

Error propagation—Standard error propagation techniques (Bevington, 1969) were used to ascertain the uncertainty in the calculated settling speed, which can be the result of uncertainty in the input parameters. Because the mathematical model's predictions are tailored for individual grains, most input parameters are measured from equatorial views of the grain in question. Not every model parameter can be provided by equatorial images. Input parameters unavailable in equatorial views, such as saccus wall thickness and grain width, are derived as an average of proximal SEM or TEM image measurements of other grains from the same species.

TABLE 1. Ultrastructural measurements of pollen grains.

Taxon	Characters				
	Thicknesses (μm)				
	Saccus wall	Exine	Intine	Endo	% Endo vs. air
Extant					
Dacrydium franklinii	0.27	0.37	0.24	2.26	19.2
Pinus strobus	0.16	0.302	0.71	2.00	24.5
Falcatifolium taxoides	0.73	1.41	0.73	Extended throughout	32.4
Fossil					
Gothania lesliana	0.918	1.24	0.75	5.42	19.9
Pteruchus fremouwensis	0.17	0.364	0.34	1.65	12.2
Pinus sp.	0.082	1.77	0.71	1.35	16.8
Caytonanthus arberi	0.20	0.65	0.71	0.53	63.3
Monoletes (from *Dolerotheca formosa*)	N/A	3.46	0.34	N/A	N/A

Note: Endo = endoreticulations; N/A = not applicable.

Stroboscopic photography—Stroboscopic photography was conducted to validate the mathematical model by empirically measuring the settling velocities of *Pinus sylvestris*, *Pinus mugho*, and *Zea mays* pollen grains. Fresh pollen grains were dropped down a cylindrical glass tube with an inner diameter of 4 cm while being illuminated by a strobe light flashing at a constant frequency of 16.67 Hz. The glass tube was covered with a plastic disk, with a small, centrally drilled hole that was aligned with the center of the tube. Tapping the grains through the hole minimized any electrostatic charges that may have been applied to the grains by the plastic disk at the top of the tube. Grains were photographed as they descended through the tube, and the trail-like trajectories were then used to calculate settling velocities. Straight pollen trails indicated there was no electrostatic interaction between the tube and the pollen grains, and, hence, no charge was transferred to the pollen. Stroboscopic photography tests were conducted at ambient temperature and relative humidity levels.

Digital imaging techniques were used to better-define the pollen trails and to help differentiate between single pollen grains and pollen clumps. First, using a function created in MATLAB (MATLAB, 2005), a "control" photograph of the empty tube was subtracted from an image of pollen falling through the tube at the same physical point in the tube. This technique removed background information from the image while leaving the pollen trail data intact. The resulting image was then thresholded, using digital imaging software (e.g., Adobe Photoshop), to create a binary image. Trails were clearly defined in the binary image, and the relative sizes of individual dots in the trails were used to separate the single grains from the clumps of pollen grains.

Aluminum stubs with double-sided tape were placed at the bottom of the tube so that pollen grains falling though the tube could be collected for analysis with the SEM. Captured pollen was measured so that its settling speed could be computationally modeled and compared to the empirically derived settling speeds measured by stroboscopic photography.

RESULTS

Structural characters—A variety of pollen structural characters were measured to use as input variables for the computational model (Table 1), which determines the terminal settling velocities of the pollen grains in this study.

Saccus wall—Most of the pollen grains had similar saccus wall thicknesses. *Gothania* and *Falcatifolium*, however, possess relatively thick saccus walls (Table 1). *Caytonanthus* had a relatively thin saccus wall (Table 1).

Exine and intine—The weighted average of exine thickness was similar for *Dacrydium* and *Pinus* (Table 1). Of the fossil pollen grains, *Pteruchus* had an exine thickness closest to the extant grains. *Gothania*, fossil *Pinus*, and *Monoletes* had the thickest exine (Table 1). Intine thicknesses of *Pinus* and *Falcatifolium* pollen grains were similar (Table 1).

Endoreticulations—The degree to which the endoreticulations extended into the saccus was quite variable among the pollen grains studied. *Falcatifolium* differed from the other grains in that its endoreticulations extended throughout the sacci (Table 1). The percentage of endoreticulations vs. air for the saccate grains was also quite variable. *Caytonanthus* possessed the highest percentage (Table 1).

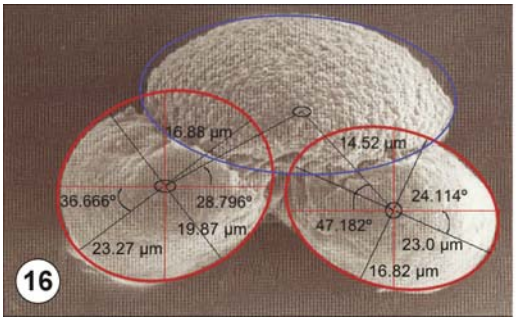

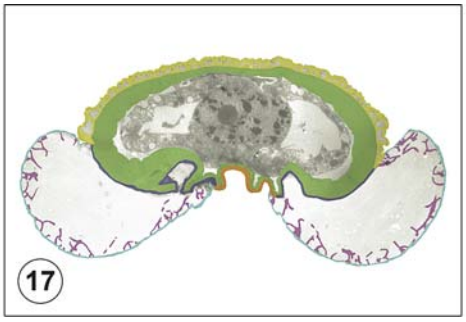

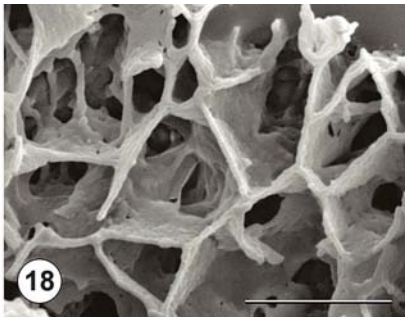

Figs. 16–18. Electron micrographs showing how pollen grains were measured. **16.** Equatorial view of a pollen grain of *Pinus strobus* with ellipses fitted to the main body (blue) and sacci (red). Note the overlap created by the three ellipses. The numbers indicate the lengths across the ellipses and the angles of rotation of the sacci. SEM. **17.** Equatorial view of a pollen grain of *P. strobus* showing the ultrastructural characters measured: proximal exine (yellow), exine at the base of the saccus (dark blue), distal exine (orange), exine of the outer saccus wall (light blue), exine of the endoreticulations (purple), and intine (green). TEM. **18.** Endoreticulations inside the saccus of a *P. strobus* pollen grain. SEM, bar = 5 μm.

Figs. 19–21. Electron micrographs and mathematically modeled pollen grain of *Pinus strobus*. **19.** Equatorial view of *P. strobus* pollen grain. SEM. **20.** Model of the pollen grain in Fig. 19. **21.** The mathematically modeled pollen grain overlaid onto the actual pollen grain. The modeled grain has been slightly scaled down in size to show the fit of the modeled grain.

Validation of the mathematical model—*Stroboscopic photography and modeled pollen*—Pollen grains of several species of *Pinus* and *Zea* were modeled, and the predicted settling speeds were compared to those empirically determined by stroboscopic photography (Table 2). The settling velocities measured using stroboscopic photography supported and validated the mathematical model's predictions. Independent sample *t* tests compared settling velocities for pollen of *P. sylvestris*, *P. mugho*, and *Z. mays* from stroboscopic photography to predictions made by the model. For each taxon, the mean prediction from the computational model did not differ from the mean empirical settling velocity ($P > 0.38$ in all cases). Thus, the model's predictions were not statistically different from empirically measured values (Table 2).

Comparisons between *Z. mays* and *Pinus* pollen grains indicate the model effectively distinguishes between pollen grains of different sizes. For instance, when statistically significant differences were found between settling speeds for *Z. mays* and *Pinus* species ($P < 0.0001$), statistically significant differences were also found between the computational model's predictions ($P < 0.02$).

Comparison of modeled pollen to published settling speeds—The model predicted a settling speed for *P. strobus* pollen of 3.07 ± 0.31 cm/s, whereas Niklas and Paw U (1983) reported a value of 2.1 cm/s for this species. Standard deviations were not available for the *P. strobus* grains reported in Niklas and Paw U (1983); therefore, the difference between the two values could not be statistically assessed. However, the model's predictions for two other species of *Pinus* (*P. sylvestris* and *P. mugho*) were validated by stroboscopic data from this study (Table 2).

An additional factor to consider with stroboscopic photography is that the drag force experienced by objects with low Reynolds numbers is increased by the proximity of walls (Vogel, 1994). For example, a cylinder with a 2-cm radius has a 0.67% impact on the actual settling velocity. This correction was considered when evaluating results from the stroboscopic experiments in this investigation, and the empirical data continue to validate those of the computational model. However, the degree of this ''wall effect'' on the reported settling speeds in other published stroboscopic studies is unknown.

The settling velocities for *Z. mays* grains predicted by the computational model and measured using stroboscopic photography differed from the settling velocities previously reported (Aylor, 2002) using similar methods (Table 2). However, this difference was due to differences in grain sizes. The pollen grains modeled in this study averaged 73.9×60.4 μm. When additional pollen was modeled using the grain dimensions reported by Aylor (2002; 90 μm in diameter), the computational model predicted a settling speed of 26.3 cm/s, which is statistically similar to Aylor's (2002) findings.

Flight orientation—Micrograph analysis of the pollen grains from the stroboscopic photography experiments indicate that saccate pollen grains fall with their sacci pointing upward (i.e., backward relative to wind direction). Of the 103 pollen grains that were not in clumps, 92 landed with their sacci pointing upward. This validates the model's assumption of orientation and its choice of drag coefficients.

When modeling flight characteristics of a pollen grain main body without sacci, questions of flight orientation are more difficult to resolve. Objects with symmetric density distributions have no preferred orientation in low Reynolds number flows (Vogel, 1994), but protrusions or asymmetries create a preferred orientation. The main body without sacci is modeled by a symmetric ellipsoid, but few real pollen grains have a completely symmetric main body. Main body settling speeds predicted by the model (Table 3) represent the average of speeds calculated using the long axis of the main body both perpendicular and parallel to the direction of motion. In no case did the orientation of the main body affect the qualitative distinction as to whether the main body alone would fall faster or slower than the pollen grain with sacci.

Reynolds numbers—The Reynolds number is a dimensionless ratio of inertial forces to viscous forces. At high Reynolds numbers, inertial forces dominate; at low Reynolds numbers, viscous forces dominate. In general, pollen grains have very low Reynolds numbers (Vogel, 1994). Because of their low Reynolds numbers and small mass, pollen grains reach their terminal velocity almost immediately. The drag coefficients used in this computational model are valid only at low Reynolds numbers (less than 1.0). The Reynolds numbers of all of the pollen grains studied here are sufficiently small, except for *Monoletes* (Table 3). However, the Reynolds number for *Monoletes* pollen is still within the range for which the mathematical model approximates a correct terminal settling velocity for this grain type (Clift et al., 1978).

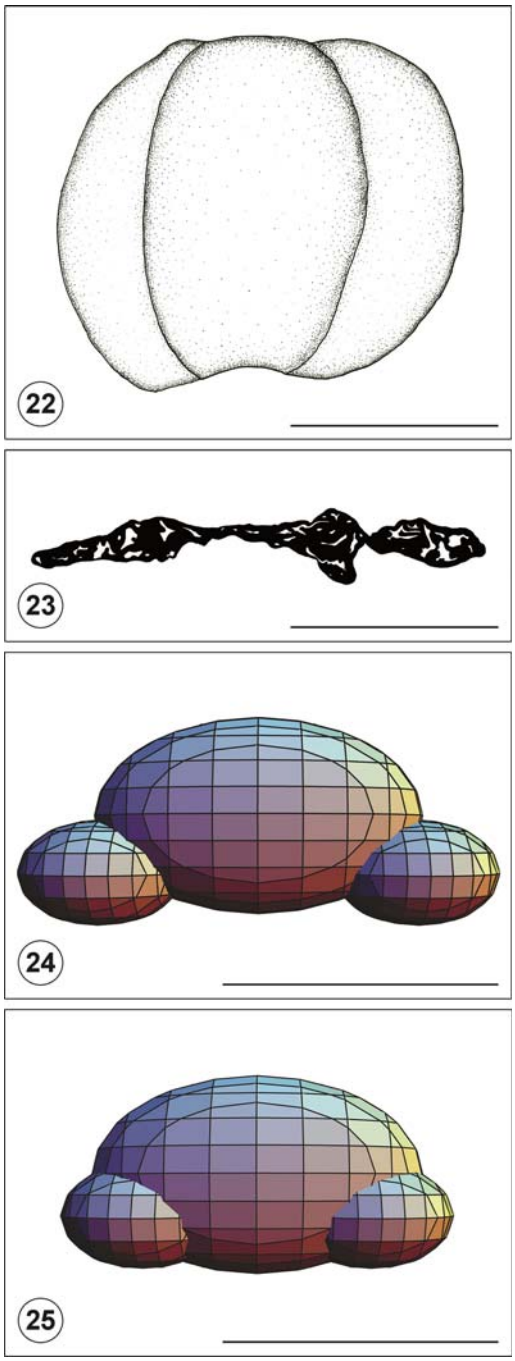

Figs. 22–25. Illustrations and mathematical models of the compressed, bisaccate pollen grain of *Caytonanthus arberi*. Bars = 10 μm. **22.** Proximal view of *Caytonanthus* pollen grain (Modified from Osborn, 1994). **23.** Equatorial section of a *Caytonanthus* pollen grain. Note the distorted shape of the pollen grain (modified from Osborn, 1994). **24.** Model of the *Caytonanthus* pollen grains shown in Figs. 22 and 23. In this model, the pollen grain has been reconstructed with minimal overlap of the sacci and main body. **25.** Model of the *Caytonanthus* pollen grains in Figs. 22 and 23. In this model, the pollen grain has been reconstructed with more overlap of the sacci and main body.

Model predictions—*Extant pollen*—The computational model predicts that a *Pinus* grain would fall faster without sacci, at 3.40 cm/s (Table 3), thereby tending to decrease its dispersal distance. The model shows the same result for pollen grains of *Dacrydium*, although the difference between the settling speeds is smaller. When modeled, the settling speed is 1.22 cm/s with sacci and 1.29 cm/s without (Table 3). This pattern does not hold for *Falcatifolium* pollen grains. For *Falcatifolium*, the modeled settling speed of a grain is 2.57 cm/s with sacci and 2.20 cm/s without (Table 3), which indicates that the pollen would be dispersed farther without sacci.

Fossil pollen—Three permineralized taxa with saccate pollen were studied using the computational model (Figs. 26–31, Table 3). The settling speed for fossil *Pinus* grains, similar to extant *Pinus* pollen, increased from 2.67 to 3.24 cm/s when the sacci were removed in the model (Table 3). This supports the idea that sacci help to increase dispersal distance of *Pinus* pollen. Bisaccate pollen of *Pteruchus* gave the same results as that of fossil *Pinus* sp. (Table 3); sacci helped to increase dispersal distance. For *Pteruchus*, the settling speed of pollen was 1.88 cm/s with sacci and 2.16 cm/s without sacci. The settling speed of monosaccate pollen of *Gothania* increased from 8.45 to 9.98 cm/s when the saccus was removed (Table 3).

Nonsaccate *Monoletes* pollen grains are large (Figs. 32–33), which contributes to their rapid settling speed of 140 cm/s (Table 3). The model-predicted settling speed of the *Monoletes* grains is more than one order of magnitude greater than the largest of the other settling speeds calculated in this study.

Caytonanthus pollen grains were mathematically expanded to three dimensions in order to accurately study them. The computational model was run under two scenarios to determine how estimating the displacement of the sacci affected the pollen. With a small amount of overlap between sacci and main body (Fig. 24), the settling speed was calculated to be 0.394 cm/s (Table 3). When more overlap was estimated (Fig. 25), the settling speed was calculated to be 0.402 cm/s (Table 3). After theoretical removal of the sacci, the calculated settling speed was 0.368 cm/s (Table 3), indicating that the modeled pollen grain dispersed farther without sacci.

Influence of structural characters on extant pollen—The mathematical model has also been used to determine how key structural characters of pollen grains affect settling speed. Three-dimensional graphs were created by plotting settling speed (the dependent variable) against two structural components as independent variables.

Plotting main body size against saccus size (Figs. 34, 35) shows similar changes in settling speed for *Pinus* and *Dacrydium*. In *Pinus* and *Dacrydium*, holding the sacci size constant as the main body size increases causes settling speed to increase (Figs. 34, 35), thereby decreasing dispersal distance. If the size of sacci is increased while the main body is held constant, the settling speed decreases. If both are increased, the settling speed still increases (Figs. 34, 35). By contrast, as the sacci of *Falcatifolium* grains are enlarged, the settling speed increases (Fig. 36), thereby decreasing dispersal distance. This phenomenon may be more clearly seen in Fig. 39.

The mathematical model has also shown that the influence of increased sacci size on the settling speed depends on the amount of endoreticulations within the sacci. Pollen grains of the three extant genera had different settling characteristics

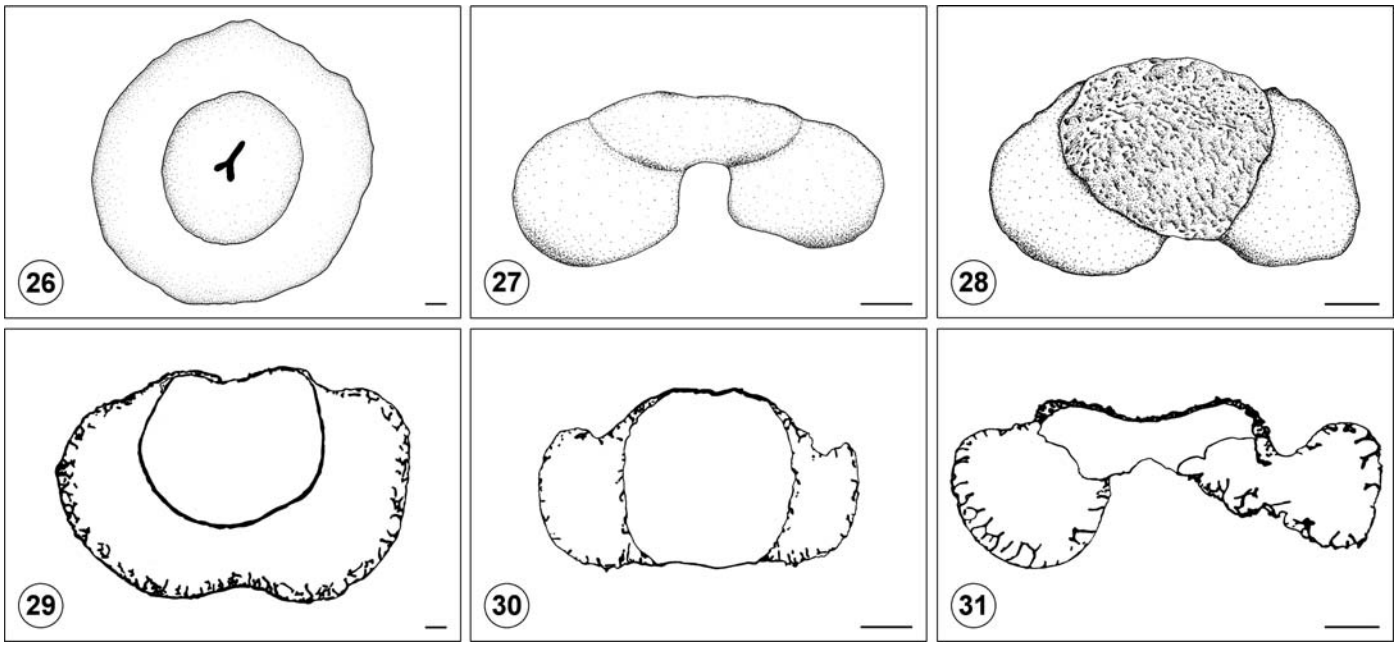

Figs. 26–31. Illustrations of the permineralized, saccate pollen grains studied. Bars = 10 μm. Fig. 26. Proximal view. Figs. 27, 29–31. Equatorial views. Fig. 28. Proximal–equatorial view. **26.** Monosaccate pollen of *Gothania lesliana* (modified from Millay and Taylor, 1976). **27.** Bisaccate pollen of *Pteruchus fremouwensis* (modified from Osborn and Taylor, 1993). **28.** Bisaccate pollen *Pinus* sp. (modified from Phipps et al., 1995). **29.** Equatorial section of a monosaccate *Gothania* pollen grain (modified from Millay and Taylor, 1976). **30.** Equatorial section of a bisaccate *Pteruchus* pollen grain (modified from Osborn and Taylor, 1993). **31.** Equatorial section of a bisaccate *Pinus* pollen grain (modified from Phipps et al., 1995).

when sacci size and percentage of endoreticulations within the sacci were varied (Figs. 37–39). In *Pinus* and *Dacrydium*, when the proportion of endoreticulations was held constant and the sacci were increased, the settling speed decreased (Figs. 37, 38). If the size of the sacci was held constant and the proportion of endoreticulations was increased, the settling speed increased as well (Figs. 37, 38). In *Falcatifolium*, when the proportion of endoreticulations was held constant and the sacci size was increased, the settling speed increased (Fig. 39). In contrast, when the proportion of endoreticulations was decreased and the sacci size was increased, the settling speed decreased (Fig. 39). These graphs explain the counterintuitive behavior of *Falcatifolium,* in which increases in sacci size did not decrease terminal velocity.

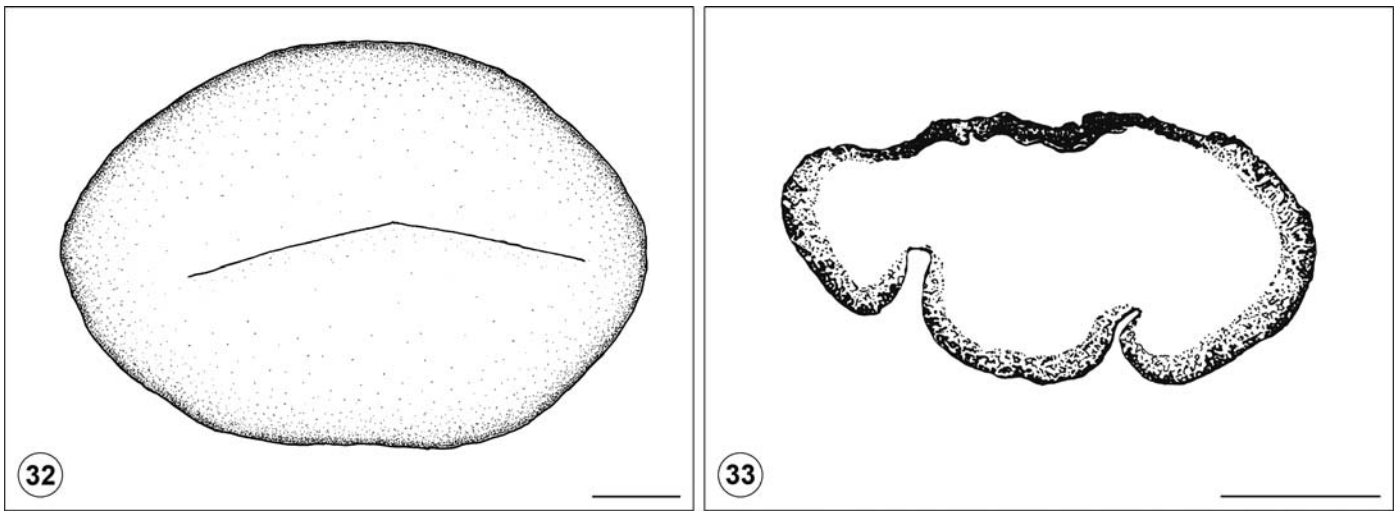

Figs. 32, 33. Illustrations of the permineralized, nonsaccate pollen of *Monoletes* (from *Dolerotheca formosa*). **32.** Proximal view of *Monoletes* pollen grain (modified from Taylor, 1978). Bar = 50 μm. **33.** Transverse section of *Monoletes* pollen grain. Note the spongy-alveolate exine (modified from Taylor, 1978). Bar = 50 μm.

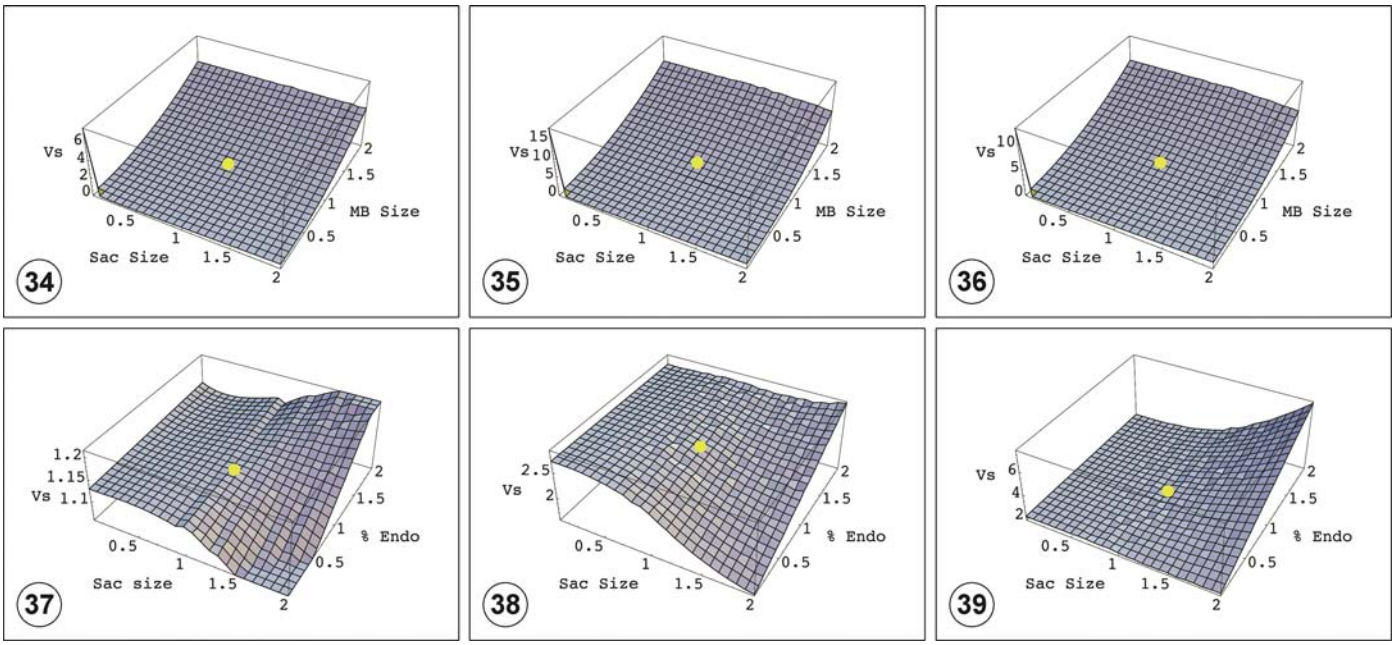

Figs. 34–39. Modeled effects of three pollen characters on terminal settling velocity on the three extant pollen types studied. Settling velocity (Vs) is shown on the vertical axis, and the characters are shown on the horizontal axes: saccus (Sac) size, main body (MB) size, and percentage of endoreticulations (% Endo). Centers of the horizontal axes (1, 1, *z*) are indicated by a yellow dot and represent an actual pollen grain studied. Note that the vertical axis scales values differently among graphs, and the values for the independent variables are scaled factors, not measures. Figs. 34–36. Effects of saccus size and main body size on settling velocity of **34.** *Dacrydium franklinii*, **35.** *Pinus strobus*, and **36.** *Falcatifolium taxoides*. Figs. 37–39. Effects of saccus size and amount of endoreticulations on settling velocity of **37.** *D. franklinii*, **38.** *P. strobus*, and **39.** *F. taxoides*.

DISCUSSION

Role of sacci in wind dispersal—*Increasing dispersal distance*—For the pollen grains of *Pinus*, *Dacrydium*, *Gothania*, fossil *Pinus*, and *Pteruchus*, the presence of sacci decreased the model-predicted settling speed, which would allow grains to disperse farther. Sacci add a significant amount of surface area to these pollen grains, increasing drag, but add a relatively small amount of mass. The small amount of added mass is due both to the relatively small amount of endoreticulations and the thin saccus wall in these five taxa. If the amount of endoreticulations in *Pinus* pollen was increased, an increased settling speed would result (Fig. 38).

The sacci on pollen grains of *Dacrydium* were very small and not large enough to influence settling speeds. For *Dacrydium* pollen, however, a decrease in settling speed does not require a large decrease in the amount of endoreticulations or a large increase in the size of the sacci (Fig. 37). These relationships corroborated results indicating the small difference between modeled settling speeds of the grain with and without sacci (Table 3). This difference was most likely due to the relatively small size of the sacci in *Dacrydium* pollen.

Model predictions for *Gothania* grains also indicate that the saccus contributed to a decrease in settling speed and an increase in dispersal distance.

TABLE 2. Settling speeds predicted by the model and empirically derived from stroboscopic photography.

Taxon	Settling speeds (cm/s)		
	Mathematical model's prediction	Stroboscopic photography	
		This study	Literature
Pinus strobus	3.07 ± 0.31	–	2.1[a]
P. sylvestris	2.97 ± 0.306	3.38 ± 0.67	–
P. mugho	2.73 ± 0.315	3.11 ± 0.81	–
Zea mays	13.68 ± 1.21	13.96 ± 2.37	30.96[b], 26[c], 26.7[c], 27.5[c]

Note: Variance reported is the standard deviation.
[a] Niklas and Paw U, 1983.
[b] Di-Giovanni et al., 1995.
[c] Aylor, 2002.

TABLE 3. Predicted terminal settling velocities for extant and fossil pollen grains modeled with and without sacci, and Reynolds numbers.

Taxon	Settling speeds (cm/s)		Reynolds numbers
	With sacci	Without sacci	
Extant			
Dacrydium franklinii	1.22 ± 0.10	1.29 ± 0.12	2.3×10^{-2}
Pinus strobus	3.07 ± 0.31	3.40 ± 0.37	1.1×10^{-1}
Falcatifolium taxoides	2.57 ± 0.24	2.20 ± 0.27	7.9×10^{-2}
Fossil			
Gothania lesliana	8.45 ± 0.16	9.98	3.1×10^{-1}
Pteruchus fremouwensis	1.88	2.16	4.3×10^{-2}
Pinus sp.	2.67	3.24	6.5×10^{-2}
Monoletes (Dolerotheca formosa)	N/A	140	2.5×10^{1}
Caytonanthus arberi			
Less overlap	0.394	0.368	1.9×10^{-3}
More overlap	0.402	0.368	1.9×10^{-3}

Note: The standard deviations come from the averaged settling speeds of several individual pollen grains. N/A = not applicable.

Decreasing dispersal distance—For pollen grains of *Falcatifolium* and *Caytonanthus*, the thickness of the saccus wall and/or the large amount of endoreticulations in the sacci cause the pollen grain to fall faster than it would if it did not have sacci. The endoreticulations in *Falcatifolium* pollen span the entirety of the sacci cavities and are thicker than endoreticulations in the other taxa studied. As a consequence, *Falcatifolium* sacci are extensively filled with sporopollenin, which adds considerable mass to the pollen. When the amount of endoreticulations in *Falcatifolium* was computationally decreased, increasing the size of the sacci did reduce the settling speed as in other taxa (Fig. 39). The increase in the saccus size or decrease in the proportion of endoreticulations needed to reduce settling speed were consistent with the large difference between the settling speeds of *Falcatifolium* grains modeled with and without sacci (Table 3).

Model-predicted results for *Caytonanthus* pollen also show a decreased settling speed when sacci are removed (Table 3). This result is due to the robust thickness of endoreticulations in *Caytonanthus* sacci, which collectively contributes to increased grain mass. In *Caytonanthus* pollen, the endoreticulations do not extend all the way through the saccus cavity as they do in *Falcatifolium*, and the saccus wall is thinner than that of *Falcatifolium*.

Monoletes—The pollination syndrome of *Monoletes*-producing plants has been hypothesized to be wind-pollinated, animal-pollinated (Taylor and Millay, 1979), or gravity-pollinated (Niklas, 1992). Although the wind-pollination hypothesis is partially supported by an alveolate pollen wall, the spongy-alveolate exine in *Monoletes* is ultrastructurally different from the platelike alveolate exine of wind-pollinated conifer and cycad pollen. The rapid settling speed of *Monoletes* pollen also indicates that this particular pollen grain was unlikely to have been wind-dispersed. The spongy-alveolate wall may have been a repository for chemicals secreted by the tapetum. These chemicals may have been similar to pollenkitt and may have facilitated animal pollination.

Effects of desiccation and pollen shape on drag—The amount of drag that acts on the pollen grain is related to the overall shape of the pollen grain (Niklas, 1992), and pollen shape can change with the grain's hydration states (Blackmore and Barnes, 1986). For example, when desiccated, the sacci of most conifer pollen grains close in around the aperture, protecting against dehydration. The longer the pollen grain spends in the air after it has dehisced, the more susceptible the grain is to water loss. Desiccation can cause a pollen grain to change its shape or orientation in flight, affecting the amount of drag on the pollen grain and consequently the settling speed (Vogel, 1994; Niklas, 1992). The shape of the grain as it travels through the air and the face of the pollen grain exposed to the moving air both influence the magnitude of the drag acting upon the grain. These shapes and orientations are crucial components of the mathematical model's predictions of pollen settling speeds. By using a coefficient that accurately depicts the amount of drag on the pollen grain under a variety of hydration states, the model can correctly estimate accurate pollen flight as hydration changes.

Surface ornamentation—Surface ornamentation may provide lift for the pollen grain, as is the case for dimples on a golf ball. However, the aerodynamic effects of surface ornamentation are often ignored when pollen grains are discussed because of their low Reynolds numbers and the difficulties with quantifying surface ornamentation. At the low Reynolds numbers of pollen grains, viscous forces of the air are thought to dominate the aerodynamic behavior of the grains (Vogel, 1994; Niklas, 1992). Many authors have stated that surface ornamentation can be ignored for objects with low Reynolds numbers (Vogel, 1994). Other authors, however, have suggested that surface ornamentation should decrease the settling velocity (Gregory, 1973; Niklas, 1985a). This decrease could result from increased lift or reduced density of the pollen grain. Bolick (1990) hypothesized that surface ornamentation can affect pollen settling velocity if the degree of roughness surpasses some theoretical threshold. Even though Vogel (1994) has stated that the aerodynamic influence of surface ornamentation at low Reynolds numbers should not have an impact according to conventional considerations, he has also stated that there is evidence in the literature (e.g., Zeleny and McKeehan, 1910) that the difference between measured settling speeds and those predicted by Stokes' Law is large enough to warrant investigating this phenomenon.

The effects of surface ornamentation on pollen flight have not yet been incorporated into the mathematical model. For a modeled pollen grain that has a slower settling speed without its sacci, the surface ornamentation of the grain could dramatically change the conclusions about the flight properties of the grain.

Conclusion—This study is the first to quantitatively demonstrate the adaptive significance of sacci for the aerodynamics of wind pollination. Sacci do function to decrease the settling speed of pollen grains, with some notable exceptions. These exceptions include pollen grains containing robust and/or extensive endoreticulations, as well as those with thick saccus walls.

The mathematical model is also important in paleobotany and in understanding the reproductive biology of key groups. This study showed that *Monoletes* pollen grains fall much too rapidly to be adequately dispersed by wind. *Gothania* pollen also settled faster than the other saccate grains. This investigation has demonstrated that compressed pollen grains can be mathematically expanded to allow for more in-depth study and analysis. The new mathematical model has also been shown to yield valid results even when sample sizes are small, which facilitates the study of fossil pollen grains. Error propagation analysis indicates that the unavoidable uncertainties associated with measurements of fossil pollen are not large enough to prohibit drawing meaningful conclusions from their modeled settling speeds.

Finally, it is clear from the current study that the structure and function of pollen sacci are the result of intense selection. Sacci are now known to serve both aerodynamic and buoyancy roles among the extant and extinct seed plants that produce saccate pollen.

LITERATURE CITED

ALMKVIST, G., AND B. BERNDT. 1988. Gauss, Landen, Ramanujan, the arithmetic–geometric mean, ellipses, #, and the ladies diary. *American Mathematical Monthly* 95: 585–608.

AYLOR, D. E. 2002. Settling speed in corn (*Zea mays*) pollen. *Journal of Aerosol Science* 33: 1601–1607.

BEVINGTON, P. 1969. Data reduction and error analysis for the physical sciences. McGraw-Hill, New York, New York, USA.

BLACKMORE, S., AND S. H. BARNES. 1986. Harmomegathic mechanisms in pollen grains. *In* S. Blackmore and I. K. Ferguson [eds.], Pollen and spores: form and function, 137–149. Academic Press, London, UK.

BOLICK, M. R. 1990. The pollen surface in wind-pollination with emphasis on the Compositae. *In* M. Hesse and F. Ehrendorfer [eds.], Morphology, development, and systematic relevance of pollen and spores, 39–51. Springer-Verlag, Wien, Austria.

CLIFT, R., J. R. GRACE, AND M. E. WEBBER. 1978. Bubbles, drops and particles. Academic Press, New York, New York, USA.

CRANE, P. R. 1986. Form and function in wind dispersed pollen. *In* S. Blackmore and I. K. Ferguson [eds.], Pollen and spores: form and function, 179–202. Academic Press, London, UK.

DI-GIOVANNI, F., P. G. KEVAN, AND M. E. NASR. 1995. The variability in settling velocities of some pollen and spores. *Grana* 34: 39–44.

DOWDING, P. 1987. Wind pollination mechanisms and aerobiology. *International Review of Cytology* 107: 421–437.

DOYLE, J., AND M. O'LEARY. 1935. Pollination in *Pinus*. *Scientific Proceedings, Royal Dublin Society* 21: 181–190.

GREGORY, P. H. 1973. The microbiology of the atmosphere. Leonard Hill, New York, New York, USA.

IMAGEJ. 2004. ImageJ software: image processing and analysis in Java. National Institutes of Health, Bethesda, Maryland, USA. Website http://rsb.info.nih.gov/ij/ [accessed June 2004].

KURMANN, M. H. 1989. Pollen wall formation in *Abies concolor* and a discussion on wall layer homologies. *Canadian Journal of Botany* 67: 2489–2504.

MATLAB. 2005. MATLAB 7.04.352 (R14), service pack 2. MathWorks, Natick, Massachusetts, USA.

MILLAY, M. A., AND T. N. TAYLOR. 1976. Evolutionary trends in fossil gymnosperm pollen. *Review of Paleobotany and Palynology* 21: 65–91.

NIKLAS, K. J. 1984. The motion of windborne pollen grains around ovulate cones: implication on wind pollination. *American Journal of Botany* 71: 356–374.

NIKLAS, K. J. 1985a. The aerodynamics of wind pollination. *Botanical Review* 51: 328–386.

NIKLAS, K. J. 1985b. Wind pollination—a study in controlled chaos. *American Scientist* 73: 462–470.

NIKLAS, K. J. 1987. Aerodynamics of wind pollination. *Scientific American* July: 90–95.

NIKLAS, K. J. 1992. Plant biomechanics: an engineering approach to plant form and function. University of Chicago Press, Chicago, Illinois, USA.

NIKLAS, K. J., AND K. T. PAW U. 1982. Pollination and airflow patterns around conifer ovulate cones. *Science* 217: 442–444.

NIKLAS, K. J., AND K. T. PAW U. 1983. Conifer ovulate cone morphology: implications on pollen impaction patterns. *American Journal of Botany* 70: 568–577.

OSBORN, J. M. 1994. The morphology and ultrastrucure of *Caytonanthus*. *Canadian Journal of Botany* 72: 1519–1527.

OSBORN, J. M., AND T. N. TAYLOR. 1993. Pollen morphology and ultrastructure of the Corystospermales: permineralized in situ grains from the Triassic of Antarctica. *Review of Paleobotany and Palynology* 79: 205–219.

OSBORN, J. M., AND T. N. TAYLOR. 1994. Comparative ultrastructure of fossil gymnosperm pollen and its phylogenetic implications. *In* M. H. Kurmann and J. A. Doyle [eds.], Ultrastructure of fossil spores and pollen, 99–121. Royal Botanic Gardens, Kew, UK.

OSBORN, J. M., T. N. TAYLOR, AND E. L. SCHNEIDER. 1991. Pollen morphology and ultrastructure of the Cabombaceae: correlations with pollination biology. *American Journal of Botany* 78: 1367–1378.

PHIPPS, C. J., J. M. OSBORN, AND R. A. STOCKEY. 1995. *Pinus* pollen cones from the Middle Eocene Princeton chert (Allenby formation) of British Columbia, Canada. *International Journal of Plant Sciences* 156: 117–124.

PRESS, W. H., B. P. FLANNERY, S. A. TEUKOLSKY, AND W. T. VETTERLING. 1986. Numerical recipes: the art of scientific computing. Cambridge University Press, Cambridge, UK.

RUNIONS, C. J., K. H. RENSING, T. TAKASO, AND J. N. OWENS. 1999. Pollination of *Picea orientalis* (Pinaceae): saccus morphology governs pollen buoyancy. *American Journal of Botany* 86: 190–197.

SALTER, J., B. G. MURRAY, AND J. E. RAGGINS. 2002. Wettable and unsinkable: the hydrodynamics of saccate pollen grains in relation to the pollination mechanism in the two New Zealand species of *Prumnopitys* Phil. (Podocarpaceae). *Annals of Botany* 89: 133–144.

SOUTHWORTH, D. 1988. Isolation of exines from gymnosperm pollen. *American Journal of Botany* 75: 15–21.

TAYLOR, T. N. 1978. The ultrastructure and reproductive significance of *Monoletes* (Pteridospermales) pollen. *Canadian Journal of Botany* 56: 3105–3118.

TAYLOR, T. N., AND C. P. DAGHLIAN. 1980. The morphology and ultrastructure of *Gothania* (Cordaitales) pollen. *Review of Palaeobotany and Palynology* 29: 1–14.

TAYLOR, T. N., AND M. A. MILLAY. 1979. Pollination biology and reproduction in early seed plants. *Review of Paleobotany and Palynology* 27: 329–355.

TOMLINSON, P. B. 1994. Functional morphology of saccate pollen in conifers with special reference to Podocarpaceae. *International Journal of Plant Sciences* 155: 699–715.

TOMLINSON, P. B. 2000. Structural features of saccate pollen types in relation to their functions. *In* M. M. Harley, C. M. Morton, and S. Blackmore [eds.], Pollen and spores: morphology and biology, 147–162. Royal Botanical Gardens, Kew, UK.

VOGEL, S. 1994. Life in moving fluids: the physical biology of flow, 2nd ed. Princeton University Press, Princeton, New Jersey, USA.

WAYNE, R., AND M. P. STAVES. 1991. The density of cell sap and endoplasm of *Nitellopsis* and *Chara*. *Plant Cell Physiology* 32: 1137–1144.

WHITEHEAD, D. R. 1983. Wind pollination: some ecological and evolutionary perspectives. *In* L. Real [ed.], Pollination biology, 97–108. Academic Press, Orlando, Florida, USA.

WODEHOUSE, R. P. 1935. Pollen grains: their structure, identification and significance in science and medicine. Hafner Publishing, New York, New York, USA.

ZAVADA, M. S. 1983. Pollen wall development of *Zamia floridana*. *Pollen et Spores* 25: 287–304.

ZELENY, J., AND L. W. MCKEEHAN. 1910. The terminal velocity of fall of small spheres in air. *Physical Review* 30: 535–560.